JPE 8-4-6

# Phase Angle Control in Resonant Inverters with Pulse Phase Modulation

Zhongming Ye†, Praveen Jain* and Paresh Sen*

†Intersil Corporation, Milpitas, CA95035, USA
*Dept. of Electrical and Electronics Eng., Queen's University, Canada

## ABSTRACT

High frequency AC (HFAC) power distribution systems delivering power through a high frequency AC link with sinusoidal voltage have the advantages of simple structure and high efficiency. In a multiple module system, where multiple resonant inverters are paralleled to the high frequency AC bus through connection inductors, it is necessary for the output voltage phase angles of the inverters be controlled so that the circulating current among the inverters be minimized. However, the phase angle of the resonant inverters output voltage can not be controlled with conventional phase shift modulation or pulse width modulation. The phase angle is a function of both the phase of the gating signals and the impedance of the resonant tank. In this paper, we proposed a pulse phase modulation (PPM) concept for the resonant inverters, so that the phase angle of the output voltage can be regulated. The PPM can be used to minimize the circulating current between the resonant inverters. The mechanisms of the phase angle control and the PPM were explained. The small signal model of a PPM controlled half-bridge resonant inverter was analyzed. The concept was verified in a half bridge resonant inverter with a series-parallel resonant tank. An HFAC power distribution system with two resonant inverters connected in parallel to a 500kHz, 28V AC bus was presented to demonstrate the applicability of the concept in a high frequency power distribution system.

**Keywords:** Resonant inverter, Pulse phase modulation, High frequency AC power distribution system, Circulating current

## 1. Introduction

High frequency alternative current power distribution systems (HFAC PDS) have been developed for a number of specific applications to deliver power to points-of-use. One example is the space power distribution architectures [1]. Other examples include airplane entertainment, engine power supply systems [2-3], contact-less power delivery systems [4-6], desktop computers and telecommunication power supply systems [7-15]. An HFAC PDS includes a front-end, a full-bridge resonant inverter (FBRI) or half-bridge resonant inverter (HBRI). The HFAC bus and AC VRM are shown in Fig.1. A resonant inverter is used to generate the HFAC sinusoidal waveform, differing from the traditional sinusoidal pulse-width-modulated (SPWM) inverters. Hence the HFAC bus frequency determines the switching frequency of the DC/AC inverters. The overall efficiency of the front-end and the inverter can be 95%, while the AC VRM can achieve efficiency of 90% or more. In order to

Manuscript received May 21, 2008; revised Aug. 12, 2008
†Corresponding Author: yezhongming@ieee.org
Tel: +1-408-546-3742, Intersil Corporation, USA
*Queen's University, Canada

increase the power density, HFAC power distribution architecture has evolved from tens of kilohertz systems to hundreds of kilohertz systems, and the 1MHz is expected to go further beyond 1MHz. The high frequency DC/AC resonant inverter is used to generate high frequency AC voltage for the HFAC bus, with features like soft-switching of the main switches and low THD in the output voltage. One half-bridge resonant inverter topology[11] is shown in Fig. 2. It consists of a half-bridge switch network, a series-parallel resonant tank, and a high frequency transformer. The feedback control includes the control error detection $K_{DV}$, a linear voltage controller $K_V$, and an asymmetrical pulse width modulator (APWM). With proper design, both switches achieve zero voltage switching. The waveform quality of the output voltage can be improved by using an additional high pass filter.

The current sharing in a HFAC system requires tight control of the phase angle of the output voltage of individual resonant inverters. Unlike the sinusoidal PWM inverters, the resonant inverters use pulse shift modulation or pulse width modulation to control the inverters. In these conventional modulation methods, the phase angle of the inverter output voltage is free of control. Therefore, even for the same pulse modulation signal, the output voltage phases can be different because of power stage diversity such as load conditions and component tolerance of the resonant and switch components. Another source of phase difference is the time delays in the control and gate drive circuits.

A pulse phase modulation concept was investigated based on the phase angle control of the output voltage of the resonant inverters. The mechanism of the pulse phase modulation will be described. Based on the topology of the half-bridge resonant inverter in Fig. 2, a phase angle controlled resonant inverter will be designed, analyzed, simulated and prototyped.

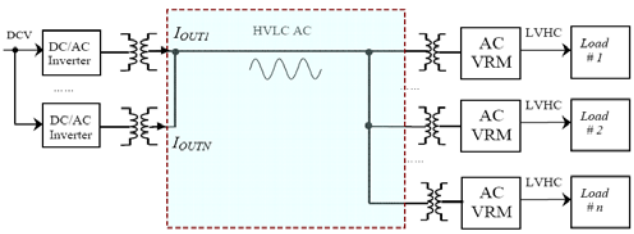


Fig. 1 Conceptual HFAC power supply system

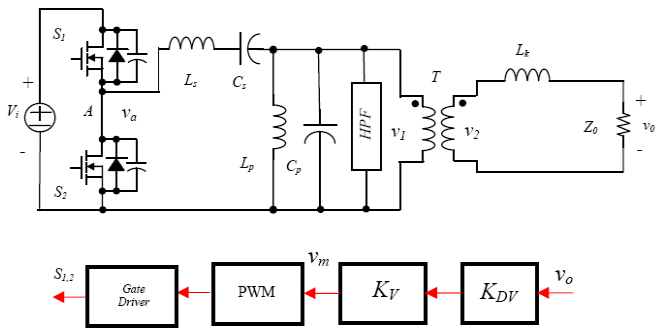


Fig. 2 Simplified schematics of a resonant inverter system

## 2. Principal Mechanism of the Pulse Phase Modulation

The phase angle of the resonant inverter is determined by the phase of the modulation pulses as well as the impedance of the equivalent load and the resonant tank. For different load conditions, the phase angles of individual inverters differ because of the component tolerances of the resonant tanks, connection inductances and gate delay time of the gate drivers. However, the phase angle between the load terminal and the bridge voltage is solely determined by the impedance of the network; such an angle is fixed for a given load condition. Therefore, by controlling the pulse phase, the phase angle of the output voltage can be regulated against the load or the line perturbation and component tolerance. In this way, the inverter behaves as a pulse phase modulated (PPM) voltage source. A PPM controlled resonant inverter is shown in Fig. 3, where the power stage is the same as the voltage controlled half-bridge resonant inverter (Fig. 2), while the control includes three basic blocks, a phase angle detector $K_D$, a phase angle controller, and a pulse phase modulator.

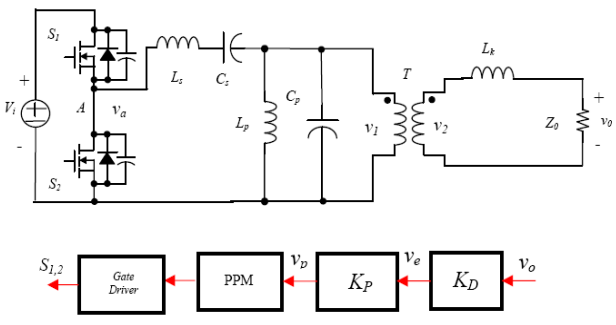

| | |
|---|---|
| $L_s$, $C_s$ | Series resonant tank inductor and capacitor |
| $L_p$, $C_p$ | Parallel resonant tank inductor and capacitor |
| $S_1$, $S_2$ | Two switches in the half bridge |
| $K_D$ | Phase angle detector |
| $K_p$ | Phase angle controller |
| PPM | Pulse phase modulator |
| $V_p$ | Phase modulation signal |
| $V_e$ | Phase error |
| $V_o$ | Output voltage |

Fig. 3 PPM controlled resonant inverter system

### 2.1 Phase angle detection

Assume the reference signal of the resonant inverter is sinusoidal with amplitude $V_r$ and phase angle $\varphi_r$ as given in (1), where $\varphi_r$ is constant, although in a current sharing control system, it is time varying and responds to the input of the controller. The output voltage of inverter $v_o$ should follow the phase of reference signal $v_r$ as closely as possible. Also assume that the filtering performance of the inverter resonant tank is so perfect that all of the harmonics are well attenuated in the inverter output terminal. Therefore, only the fundamental frequency (operation frequency) component is considered.

$$v_r = V_r \sin(\omega t + \varphi_r) \tag{1}$$

Suppose the output voltage has amplitude $V_o$ and phase angle $\varphi_o$, as represented by cosine in (2), where $\varphi_o$ is time varying during transient.

$$v_o = V_o \cos(\omega t + \varphi_o(t)) \tag{2}$$

The actual phase error $\varphi_e$ between these two signals is given in (3). Therefore, the objective of the phase angle control is to minimize the phase angle difference between the reference signal $v_r$ and inverter output voltage $v_o$ in both the steady state and transient state. From (1) and (2), apply the multiplier operation to the two signals, and the output voltage of the multiplier is derived in (4).

$$\varphi_e(t) = \varphi_o(t) - \varphi_r \tag{3}$$

$$v_e = 0.5 V_r V_o \left(\sin(-\varphi_o(t) + \varphi_r) + \sin(2\omega t + \varphi_o(t) + \varphi_r)\right) \tag{4}$$

The expression in (4) has two terms, a DC term, and an AC term, with frequency twice the switching frequency, which can be easily filtered out by a low pass filter. Therefore, if the harmonics are filtered out, then the output of the multiplier is related to the phase difference between the reference signal $v_r$ and the real inverter output voltage $v_0$ by a sinusoidal function as given in (5). It is noted that because the phase angle of the output voltage is time varying, the phase error after the low pass filter, $V_e$, is still a function of time.

$$V_e = 0.5 V_r V_o \sin(-\varphi_o(t) + \varphi_r) \tag{5}$$

The sine function can be linearized near zero. For small phase difference, $V_e$ is approximately in proportion to the phase difference by a factor $K_D$, which is the gain of the phase detector.

$$V_e(t) \approx K_D(\varphi_r - \varphi_0(t)), \ \|\varphi_r - \varphi_0(t)\| \to 0 \tag{6}$$

Hence the phase angle difference between these two signals can be easily detected with an analog multiplier and a low pass filter of cut-off frequency lower than the operation frequency of the resonant inverter.

### 2.2. Pulse phase modulation

The logic scheme for the pulse phase modulation is shown in Fig. 4(a), which consists of a DFF, a SR FF, two comparators and 2 XOR gates. The input signals to the PPM include the carrier signal $v_c$, which is a saw-tooth waveform, and the phase modulation signal $v_p$. The carrier waveform modulates the phase modulation signal and generates a PWM signal in reverse proportion to the modulation signal, which is then used to generate the gate signals.

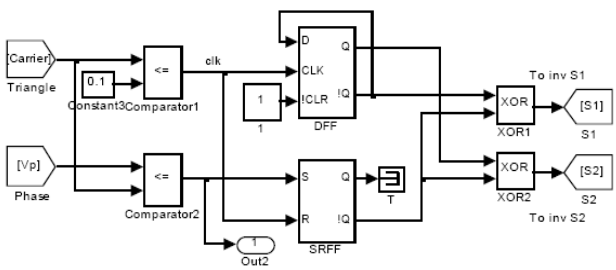


(a) The logic circuit for the PPM

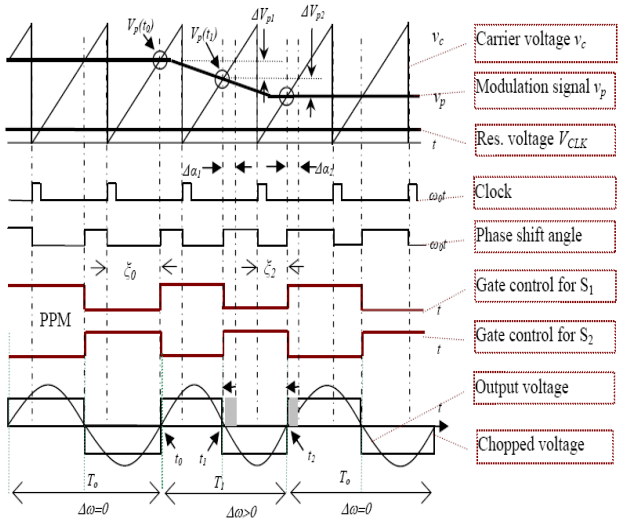


(b)Principal waveforms of the pulse phase modulation

Fig. 4 Schematic of PPM controller and the operation waveforms

The mechanism to shift the phase angle for a change of the phase angle modulation signal is explained with the operation waveforms in Fig. 4(b), where the modulation signal has a transient within one operation period. For one complete PPM pattern of period $T_0$, it needs two pulses of the carrier signal to finish. The modulation signal is assured consistency before and after the transient. The PPM for the inverter has a duty ratio of *D=0.5*. The initial phase angle with respect to the clock signal is $\xi_0$. The initial switching period is $T_0$. The phase modulation signal $v_p$ is time varying.

Let the gain $K_M$ be the change of the PPM phase angle to the modulation signal variation $\Delta v_p$, which is the slope of the carrier signal $v_c$, according to the geometry relationship in Fig. 4(b).

$$K_M = \frac{\Delta\alpha}{\Delta v_p} = \pi / V_{pp} \quad \text{or} \quad \Delta\alpha = K_M \Delta v_p \,, \tag{7}$$

$$\text{where} \quad \left\| \Delta v_p \right\| < V_{pp}$$

Assume at $t_0$ transient begins. The phase modulation signal is $v_p(t_0)$ at $t_0$. $v_p(t)$ intersects with the carrier signal $v_c$ at $t_1$. The corresponding modulation signal at $t_1$ is $v_p(t_1)$, which is given in (8).

$$v_p(t_1) = v_p(t_0) - \Delta V_{p1} \tag{8}$$

The pulse reduction $\Delta\alpha_1$ corresponding to the modulation signal change is determined by $K_M$, and is given by (9).

$$\Delta\alpha_1 = K_M \Delta V_{p1} \tag{9}$$

Then $v_p(t)$ intersects the successive pulse of the carrier signal $v_c$ at $t_2$. At $t_2$, the modulation signal is given by (10), corresponding to phase reduction $\Delta\alpha_2$ (11).

$$v_p(t_2) = v_p(t_1) - \Delta V_{p2} \tag{10}$$

$$\Delta\alpha_2 = K_M \Delta V_{p2} \tag{11}$$

Altogether, the phase angle is shifted forward by $\Delta\alpha$, which is given in (12), or in the time domain, this corresponds to the reduction of the switching period by $\Delta T$, which is given in (13), together with the new PPM period. The final phase angle with respect to the clock signal is $\xi_2$, as indicated in Fig. 4(b).

$$\Delta\alpha = K_M (\Delta V_{p1} + \Delta V_{p2}) \tag{12}$$

$$\Delta T = \frac{\Delta V_{p1} + \Delta V_{p2}}{2V_{pp}} T_0 \tag{13}$$

$$T_1 = T_0 - \Delta T = T_0 \frac{2V_{pp} - \Delta V_p}{2V_{pp}}$$

Therefore, the equivalent frequency of this switching period is different from the original one, and the increase of frequency is $\Delta\omega$, which is given in (14)

$$\Delta\omega = \omega_0 \frac{\Delta V_p}{2V_{pp} - \Delta V_p} \tag{14}$$

The corresponding equivalent frequency of the PPM for this period is increased and given in (15). After the transient, the frequency restores to the original frequency $\omega_0$.

$$\omega_{(1)} = \omega_{(0)} + \Delta\omega \tag{15}$$

The duty ratio during this transient period is time

varying, and is determined by the modulation signal variations, as is given in (16). Since $\Delta V_p$ changes from zero to $V_{pp}$, the range of the duty ratio D is from 0 to 1 during transient.

$$D_{(1)} = \frac{V_{pp} - \Delta V_{p1}}{2V_{pp} - (\Delta V_{p1} + \Delta V_{p2})} \tag{16}$$

Since the inverter can be treated as an LTI network, the frequency of the output voltage is the same as the PPM signal. Therefore, the output voltage can be written in (17) for the next period. Obviously, the phase angle of the output voltage can be controlled through the phase angle modulation signal $v_p$. The phase angle with respect to the clock signal is $\xi_2$.

$$v_o = V_o \cos(\omega_0 t + \Delta\alpha + \varphi_0) \tag{17}$$

The phase angle controller $K_p$ calculates the phase modulation signal $v_p$ from the phase error signal $V_e$ which is from the phase angle detector circuit. As long as the phase angle of the output voltage approximates that of the reference signal, the output of the phase detection will be approximately constant after a certain time. Then the frequency change of the PPM will be zero also, indicating the end of the transient.

The theoretical range of phase angle control is from 0 to π. However, it is noted that there is no interval overlap between the PWM pulse and the clock signal. And the modulation signal should be kept below the peak of carrier $v_c$. Therefore, the relationship between the modulation signal and the phase shift angle is shown in Fig. 5. $\alpha_{\min}$ is given in (18) where $V_{CLK}$ is the voltage level compared with the carrier signal and it generates the clock signal.

$$\alpha_{\min} = \frac{V_{CLK} T}{2V_{PP}} \tag{18}$$

In order to adjust the phase angle towards both positive and negative directions to π/2, it is suggested that the saw-tooth waveform rises from $-V_{pp}/2$ to $+V_{pp}/2$. Then the phase angle control range is [-π/2,π/2].

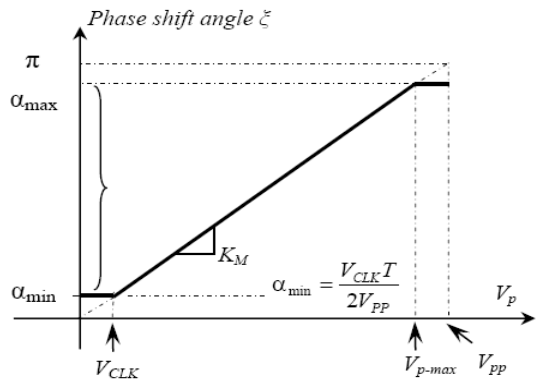


Fig. 5 Relationship between modulation signal and PPM phase shift

### 2.3 Small signal analysis

The system of the PPM controlled resonant inverter (in Fig. 3) is nonlinear because of the pulse phase modulation and the multiplier operation for the phase angle detection. It is necessary to derive a linear model so that the controller can be designed. Assume at a certain operation point the system reaches a steady state. If small perturbations and linearization are applied to the system, it can be simplified as a small signal linear system.

The phase angle error between the inverter output voltage and the reference signal is detected by a multiplier and a low pass filter in combination and represented as a voltage signal, according to (5). Around any steady state operation point, the phase difference is very small, that is, $\|\varphi_o - \varphi_r\| << 1$.

In the small signal sense the phase error is linearly related to the phase angle difference of the two signals. Therefore, the error signal or the phase modulation signal is given in (19), where $K_F(s)$ is the transfer function of the low pass filter.

$$V_e = F_F(s) K_D (\varphi_o - \varphi_r) \tag{19}$$

Since the resonant tank of the inverter has no amplification on the phase shift angle, it is treated as a unity gain unit and the impedance phase angle of the resonant tank is treated as perturbation.

The small signal model of the system is shown in Fig. 6, where $K_D$ is the gain of the multiplier, $K_p$(s) is the phase angle controller, $F_M(s)$ is the transfer function of the PPM,

$F_F(s)$ is the low pass filter. The closed loop system transfer function is hence given in (20).

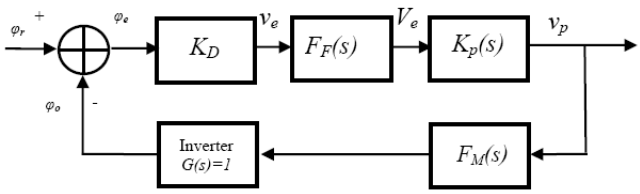


$K_D$ Phase angle detector gain
$F_F(s)$ Low pass filter transfer function
$K_p(s)$ Phase angle controller
$F_M(s)$ PPM modulator transfer function

Fig. 6 Small signal model of PPM controlled resonant inverter

$$H(s) = \frac{K_D F_F(s) K_P(s) F_M(s)}{1 + K_D F_F(s) K_P(s) F_M(s)} \tag{20}$$

The transfer function of the inverter output voltage phase angle tracking error is given by (21), from which the phase angle tracking error can be evaluated.

$$H_e(s) = 1 - H(s) = \frac{1}{1 + K_D F_F(s) K_P(s) F_M(s)} \tag{21}$$

The phase angle controller can be designed with the gain-phase margin approach. A simple design is to use a *PI* controller with proportion $K_c$ and time constant $T_c$, for the detection and control. The low pass filter can be replaced with an integral $K_F/s$. The transfer function from the input phase angle to output phase angle can be written in (22), which is a 2nd order system.

$$H(s) = \frac{K_D K_F K_c K_M s + K_D K_F K_M / T_c}{s^2 + K_D K_F K_c K_M s + F_M K_D F_F K_c / T_c} \tag{22}$$

The natural resonant frequency of the system is given in (23), and the damping factor is given in (24), which are solely determined by the controller parameters $T_c$ and $K_c$, and the integral time constant $K_F$.

$$\omega_n = \sqrt{K_M K_D}\sqrt{K_F K_c / T_c} \tag{23}$$

$$\zeta = \sqrt{K_M K_D}\sqrt{K_F K_c T_c} \tag{24}$$

The frequency responses of the PPM-controlled resonant inverter are plotted for different parameters of $K_c$, $T_c$ and $K_F$ in Fig. 7. The damping factor can be increased with large time constant $T_c$. And the bandwidth of the system can be increased with a large $K_c$.

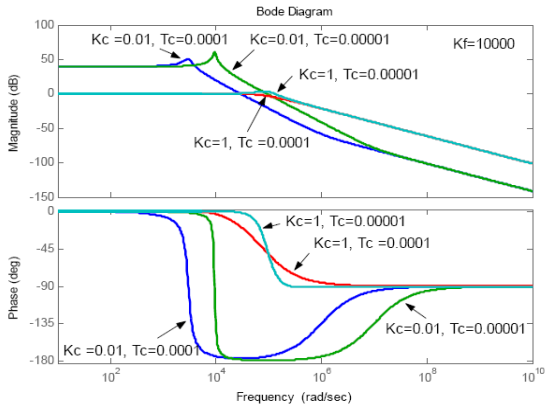


(a) $K_c$=.01, 1; $K_f$=10k

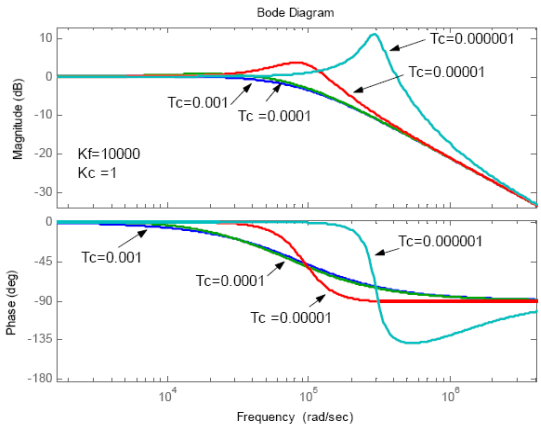


(b) $K_c$=1; $K_f$=10k; $T_c$=$10^{-3}$, $10^{-4}$, $10^{-5}$, $10^{-6}$

Fig. 7 Frequency domain response of the PPM-controlled system

## 3. PPM-controlled Half-bridge Resonant Inverter

A PPM-controlled half-bridge (HB) series-parallel resonant inverter as shown in Fig. 3 is designed. The input to the HB resonant inverter module is 38V. The two switches in the half bridge are driven by complementary gate signals of frequency 500 kHz. To prevent a short in the DC source, enough dead time is mandatory. The output power of the inverter is 100W. The output voltage is 500 kHz sinusoidal with amplitude 39V (Peak). A high frequency transformer of turns-ratio 1:2.2 is used. $L_s$= 3.9 μH, $C_s$ = 27nF; $L_p$ =

0.98μH, $C_p$ = 85 nF

The resonant tank not only filters out the harmonics in the semi-square voltage, but also offers soft-switching for the power switches. A resonant tank with two energy storage components is usually used in DC/DC conversion topologies, for example, the parallel resonant converter and the series resonant converter. A sinusoidal voltage waveform with very small THD is desirable in an HFAC system to avoid Electromagnetic Interference (EMI) in the HFAC bus. The series-parallel resonant tank with four energy storage components gives more design freedom in the soft-switching design. Such a resonant tank also has better filtering performance than an LCC or LC tank. Therefore, it is a reasonable choice for HFAC applications. In Fig. 3, $L_s$ and $C_s$ are the series resonant network inductor and capacitor, respectively. $L_p$ and $C_p$ are the parallel resonant network inductor and capacitor, respectively. The resonant frequencies of the series and parallel resonant tank are determined by the series and parallel inductor and capacitors as given in (25).

$$\omega_s = 1/\sqrt{L_s C_s}\,; \qquad \omega_p = 1/\sqrt{L_p C_p} \tag{25}$$

The series resonant tank is tuned to above 0.95 of the operation frequency. The parallel resonant tank is tuned to 1.2 of the operation frequency. Therefore, the impedance viewed from the input port of the resonant tank is inductive at operation frequency. Since the pulses are symmetrical, there is no even order harmonics in the chopped voltage. Therefore, no high order filter is needed.

The impedance viewed from the input port of the resonant network depends on both the parameters of the resonant tank and equivalent load of the HFAC bus, and is given in (26), where $Z_s$ and $Z_p$ represent the impedances of the series resonant tank and parallel resonant tank, respectively.

$$Z_{ih} = Z_{sh} + Z_{ph} \tag{26}$$

The impedance of the series and parallel resonant tanks are given in (27) and (28), respectively, in which the equivalent resistance $R_e$ and equivalent reactance $X_e$ are the equivalent load impedances of the HFAC bus reflected from the secondary side of the transformer to the primary side.

$$Z_{sh} = R_s + j(hX_{Ls} - X_{Cs}/h) \tag{27}$$

$$Z_{ph}^{-1} = \frac{R_e}{R_e^2 + X_{eh}^2} + j\left(\frac{h}{X_{Cp}} - \frac{1}{X_{Lp}h} - \frac{X_{eh}}{R_e^2 + X_{eh}^2}\right) \tag{28}$$

In a general case with a non-resistive equivalent load of the AC bus, the AC gain of the resonant tank $A_h$ is given in (29).

$$A_h = \left\| \frac{Z_{p,h}}{Z_{s,h} + Z_{p,h}} \right\| = \left( \frac{R_{p,h}^{\ 2} + X_{p,h}^{\ 2}}{(R_s + R_{p,h})^2 + (X_{s,h} + X_{p,h})^2} \right)^{1/2} \tag{29}$$

In the above, $R_{p,h}$ is the equivalent resistance of the parallel resonant tank, $R_s$ is the equivalent resistance of the series resonant tank, $X_{s,h}$ is the equivalent reactance of the series resonant tank, and $X_{p,h}$ is the equivalent reactance of the parallel resonant tank.

The instantaneous voltage of the primary winding of the transformer can be expressed in (30), where $\gamma_h$ is the phase difference between the bridge voltage $V_{a,h}$ and the voltage of the parallel resonant tank $V_{1,h}$ of $h^{th}$ order harmonic components, and is given in (31).

$$v_{1,h}(t) = \sum_h A_h \frac{2V_{in}}{h\pi} \sin\frac{h\pi}{2} \sin(h\omega_o t - \gamma_h) \tag{30}$$

$$\gamma_h = a\tan\frac{X_{p,h}(R_s + R_{p,h}) - R_{p,h}(X_{s,h} + X_{p,h})}{R_{p,h}(R_s + R_{p,h}) + X_{p,h}(X_{s,h} + X_{p,h})} \tag{31}$$

The phase angle difference $\Delta\gamma$ between a nominal inverter and that with a different series inductor $L_s$ (= $L_{s0}$ + $\Delta L_s$) are plotted in Fig. 8 for different load conditions. It is obvious that both the load impedance and the impedance of the resonant tank determine the value of the phase angle difference $\Delta\gamma$. For the same bridge voltage, the phase angle of the output voltage can be different because of the component tolerance of the power circuit, and the load variations.

A prototype PPM controlled half-bridge resonant inverter was built in the lab. The circuit specifications and component parameters are given in Table 1. The MOSFET devices are IRF540N. The resonant capacitors

are Wima FKP, and the magnetic core of the transformer is TDKPC44LP22/13. The thermal resistors are used in parallel as the equivalent load for the resonant inverter. The power factor of the equivalent load at the operation frequency is corrected by series connection capacitors.

Table 1 Circuit specifications and component parameters

| Specifications & Component Parameters | |
|---|---|
| Output voltage $V_o$ | 18V (Peak) |
| Input voltage $V_{in}$ | 38V (Average) |
| Frequency $f_s$ | 0.5 MHz |
| Efficiency $\eta$ | 92% |
| Output Power $P_o$ | 100W |
| Series resonant tank | $L_s$=3.9 μH, $C_s$=27nF |
| Parallel Resonant tank | $L_p$=0.98μH, $C_p$=85 nF |
| Switches | IRF540N |
| Transformer $T$ | 1:2.2, Input 18V/Output 38V |
| Core | TDKPC44LP22/13 |
| Gate drivers | HIP2101 |

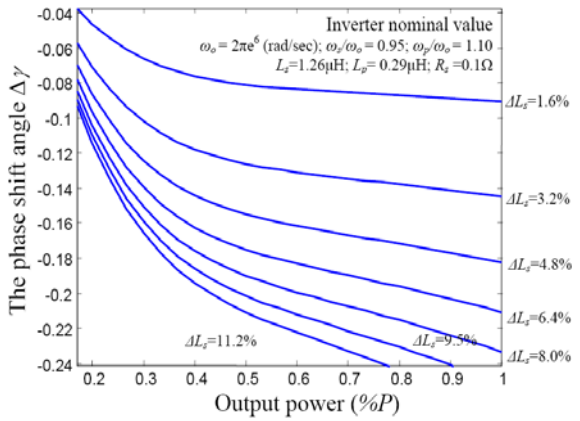


Fig. 8 Phase angle difference $\Delta\gamma = \gamma_1 - \gamma_0$, where, $\gamma_0$ is the phase shift angle of the nominal inverter ($L_{s0}$), $\gamma_1$ is that of the inverter with a different $L_s$, $L_s = L_{s0} + \Delta L_s$

The circuit diagram of the pulse phase modulation is given in Fig. 9, where the commercial available discrete components including 74F08, 74F86, and 74F74 have very small time delays. The dead time is set to 80ns by the RCD circuit.

The verification waveforms are given in Figures 10 and 11. In Fig. 10, the voltages across the drain and source of the main switches, and the currents are shown. From these waveforms, it is observed that both of the switches achieve zero voltage switching. For instance, at the instant switch $S_1$ is turned on, the resonant current is negative. Therefore, the resonant current flows in the anti-parallel diode of the switch $S_1$, and the voltage across the drain and source is clamped to zero. Therefore, $S_1$ is turned on under zero voltage. The turning off of the switches is softened with snubber capacitors. The magnetizing inductance current of the high frequency transformer offers enough current for open-load conditions.

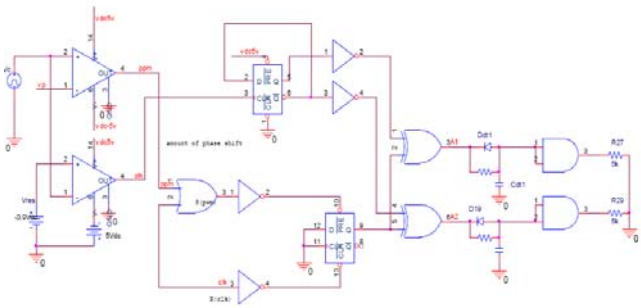

Fig. 9 Circuit diagram for the PPM

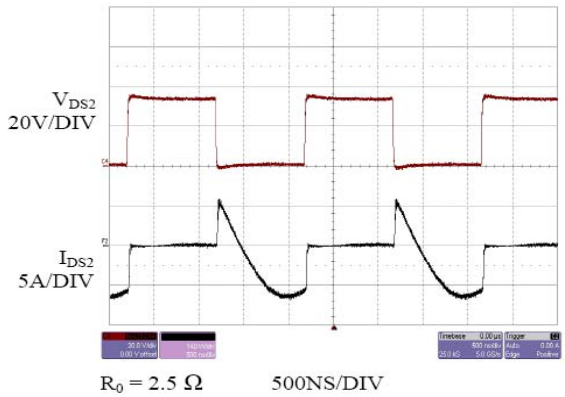


(a)

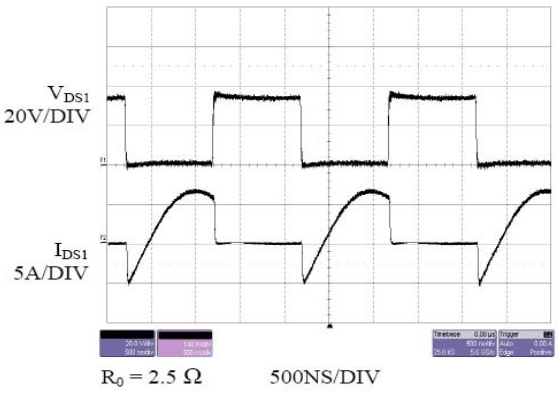


(b)

Fig. 10 Voltages and currents of the main switches (a) FET $S_2$, (b) FET $S_1$ in the second stage $R_0$ =2.5Ω

The operation waveforms for the resonant inverter with different phase modulation levels are given in Fig. 11, where the phase modulation signal, clock signal and the output voltages of the inverters are given. The top waveforms are the phase modulation signals $V_P$, the middle ones are the Clock signals Clock, which are synchronized to the same for all inverter modules, and the bottom ones are the output voltages $V_O$. For a large modulation signal ($V_P$ =0.8V), the phase angle of the output voltage with respect to the clock signal is $\xi_1 \approx$ 365ns. For a small modulation signal ($V_P$ =0.1V), the phase angle of the output voltage with respect to the clock signal is $\xi_2 \approx$ 250ns.

Obviously with the PPM control, the output voltage phase angles can be controlled through a phase angle feedback control. Some application examples of the PPM control include: synchronize the output voltage phase angles of the inverters; control the active and reactive power flow by controlling the phase angles; minimize the circulating current by combining the PPM with certain current sharing control scheme. In the next section, it will be shown through experiments that by controlling the phase angles of the output voltages of individual inverters in a multiple inverter system, the circulating current can be reduced.

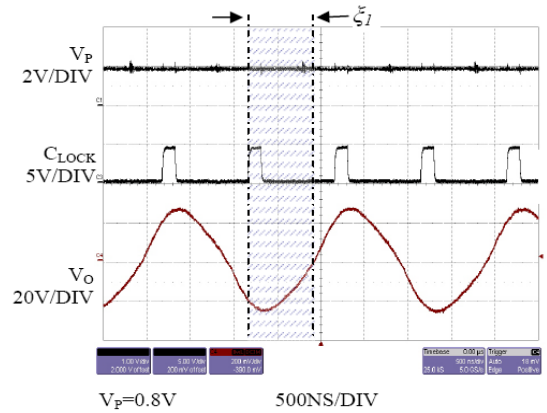


(a) $v_p$=.8V

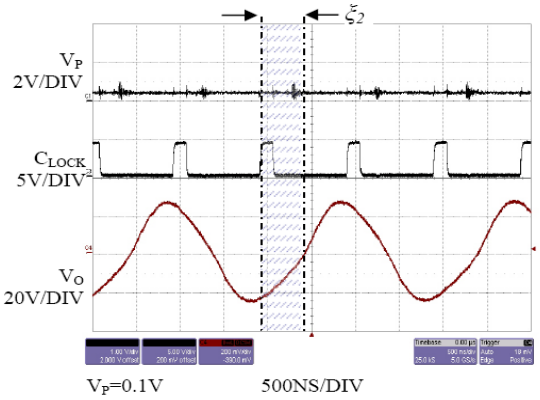


(b) $v_p$= 0.1V

Fig. 11 Waveforms for the pulse phase modulation

## 4. Two-stage Resonant Inverter with Phase and Magnitude Control

Two resonant inverter modules as shown in Fig. 12 were built in the lab to make up a two-inverter system. Each resonant inverter consists of two stages. The second stage of each resonant inverter module is the same as the half-bridge resonant inverter that we have discussed in the previous section. It operates at 500 kHz, and the output of each inverter module is 100W, 28V (RMS). To avoid the phase shift problem, this stage is not for voltage magnitude control. Since the duty ratio is kept 50%, the switches in this stage are always soft-switched. The resonant tank and the switches are optimized for minimum conduction loss. The first stage is a two-switch buck converter running at 1 MHz, and is solely for voltage magnitude control. Compared with the single-stage full-bridge topology, the two-stage provides similar efficiency, while offering much more flexibility in the topology and pulse modulation design.

Although both inverters use the same parameters, there are component tolerances. For instance, the component tolerance for the commercial resonant inductors is above 10%. The internal conduction resistance of the MOSFET can be as high as 50%.

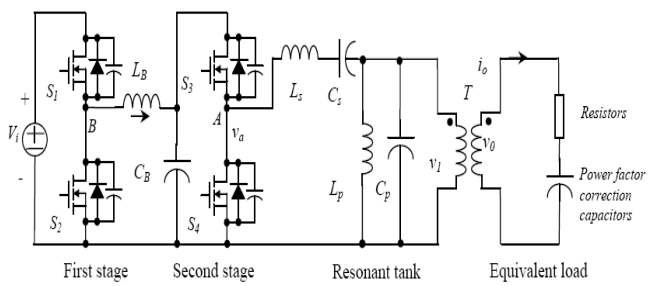


Fig. 12 Simplified circuit schematics of a 2-stage inverter system

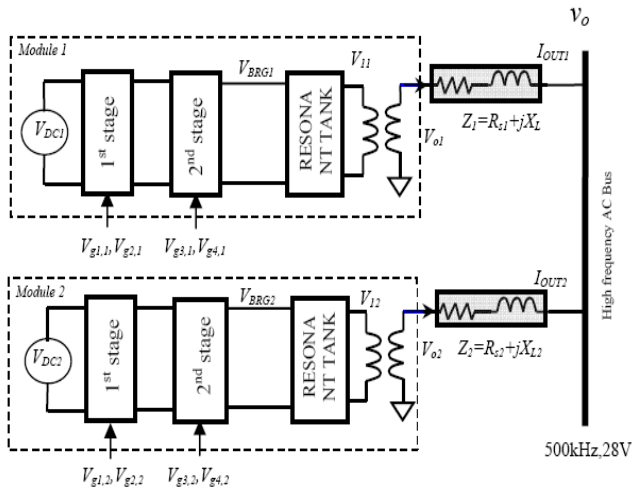


Fig. 13 Control and power stage layout of the system

The two resonant inverters are connected to the high frequency AC bus through small connection inductors. The system layout is shown in Fig. 13, where the topology of each inverter module is shown in Fig. 12. A connection inductor $Z_K$ is used and is modeled as a resistance and reactance in series, $Z_k = R_k + jX_k$. Assuming that the equivalent load of the HFAC bus is resistive, based on AC analysis, the circulating current between the two inverter modules is given in (32), where C is a coefficient, $V_{O1}$ and $V_{O2}$ are the terminal voltages of the resonant inverters, which are functions of the input voltages, impedance of the resonant tanks, and the switching functions of the switching networks, according to (30). $R$ is the equivalent load resistance of the HFAC bus.

$$\frac{2\Delta\dot{I}}{C} = 2V_{O1}\angle\phi_1 - 2V_{O2}\angle\phi_1 + j\left(\frac{Z_{K2}}{R}V_{O1}\angle\phi_1 - \frac{Z_{K1}}{R}V_{O2}\angle\phi_1\right) \quad (32)$$

Obviously, both the discrepancy of phase angles and magnitudes of the output voltages of the inverters cause circulating current. In addition, the difference in the connection inductors can also cause uneven current distribution. Therefore, paralleling multiple resonant inverters in a high frequency AC system is much more complicated than paralleling multiple converters in a DC system.

The connection inductance is critical to limit the circulating current in the HFAC power system. The size of the connection inductor should be compromised for output voltage regulation as well as for space and cost. Furthermore, the conduction resistance must be very small to minimize thermal losses. Generally, the connection inductors should meet the following conditions in (33) and (34).

$$X_{L_{K1}} \approx X_{L_{K2}} \quad (33)$$

$$X_{L_{K1}} >> R_{k1}; X_{L_{K2}} >> R_{k2} \quad (34)$$

In practice, the connection inductance consists of both the leakage inductance of the high frequency transformer, and external inductance, both of which have large component tolerance. The measured inductances are as follows: $L_1 = 0.23\mu H$, $L_2 = 0.27\mu H$. The discrepancy of the connection inductance is an important cause of circulating current, according to (32).

In order to reduce the circulating current between the inverter modules, three possibilities exist. 1) Using large connection inductors. However, this causes large voltage drop over the connection inductors. 2) Using components (including the connection inductors) with small component tolerance. This increases the cost of the system, and can not eliminate the circulating current caused by the control circuit discrepancy. 3) Using proper current sharing control with PPM.

1) Output voltage magnitude is controlled through the first stage with PWM

In the PWM-controlled inverter, the first-stage voltage is regulated through $V_{g1,n}$, $V_{g1,n}$, $n$ = 1,2. The second stage is free of control, but uses the same gate drive pulses as the other module. $V_{g3,1} = V_{g3,2}$, $V_{g4,1} = V_{g4,2}$. Because of the component tolerance in the second stage, there is phenomenal phase discrepancy between the output voltages $V_{01}$ and $V_{02}$. Together with the connection inductance difference, it will cause large circulating current. In Fig. 14(a), the DC inputs $V_{DC1}$ and $V_{DC2}$ are different. $V_{DC1}$ = 55V, $V_{DC2}$ = 75V. With the PWM control in the first stage, the first stage output voltages of both the two inverters are 38V. However, the circulating current is about 25% of the load current.

The circulating current is caused by the asymmetry existing in the second stages of the two inverter modules.

As can be seen from (31) and Fig. 8, phase discrepancy may be a result of the component tolerance of the power stage, even using the same pulses to drive the two second stages.

Another factor is the delay in the control, including the gate drive circuit, and the modulation circuit. The rising time and falling time of the commercial gate drivers change with operation conditions, like temperature, operation voltages, and output capacitances. Delay differences also exist in the modulation circuit. For example, the component tolerance in the RCD dead-time setting circuit can cause the drive pulses to differ from each other, even with the same modulation signal.

2) Output voltage phase angle is controlled with PPM

In contrast, the PPM-controlled resonant inverter regulates the phase angle of the output voltage against any possible perturbations and defects of the circuits, as shown in Fig. 14(b). The first stages are controlled with PWM control $V_{g1,n}$, $V_{g1,n}$, $n$ = 1,2. The DC voltages applied to the second stages are 38V. The magnitudes of the output voltage are, however, free of control. The second stage is PPM-controlled. The circulating current between the two modules is effectively reduced to about 12% of the load current. The remaining small current distribution error is caused by the voltage magnitude discrepancy of the two modules, and the connection inductor difference. The corresponding voltage $V_{01}$, $V_{02}$, and the gating signals $V_{g3,1}$, $V_{g3,2}$, $V_{g4,1}$, and $V_{g4,2}$ are given in Figures 15(a) and (b), respectively.

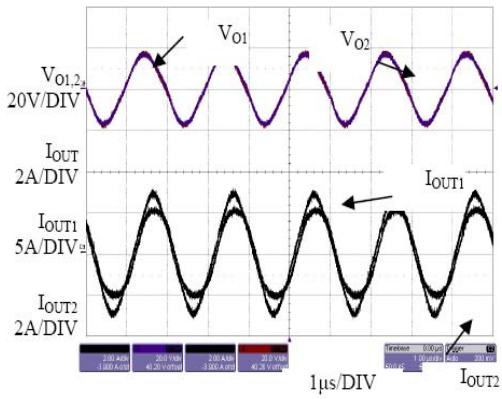


(a) Without PPM control

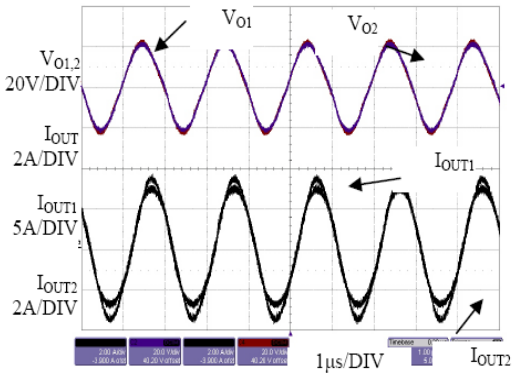


(b) With PPM control

Fig. 14 Current sharing improvement with phase angle control

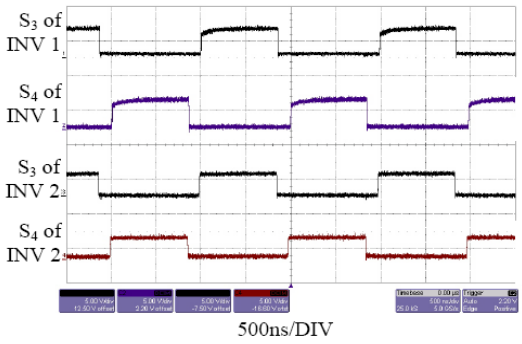


(a) Gating signals

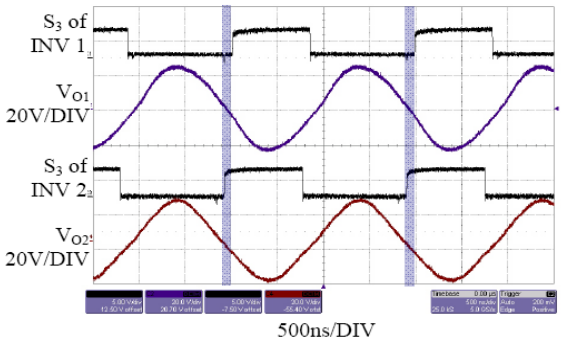


(b) Output voltages of two modules

Fig. 15 Detailed experimental waveforms of the inverters system

## 5. Conclusions

The phase angles of the output voltage of the resonant inverters are different from each other, making it very

difficult for parallel operation of multiple resonant inverters. There are mainly three factors that contribute to the phase discrepancy. 1) The phase angle of the inverter output voltage is free from control in the conventional modulation methods. Therefore, even for the same pulse modulation signal, the output voltage phases can be different because of the power stage diversity such as load conditions and component tolerance of the resonant and switch components. 2) The time delays in the control and gate drive circuits make it impossible to synchronize the pulses. 3) For all the conventional resonant inverters, the phase angle of the output voltage changes with the modulation levels of the modulators, which changes for voltage regulation. In other words, the phase angle of the output voltage is coupled with the magnitude control. The differences in the output voltage phase angles of individual inverters cause circulating currents, and decrease the system efficiency. In order to reduce the circulating currents, effective control of the phase angle of the resonant inverter is expected.

A pulse phase modulation concept was proposed for the resonant inverter, so that the phase angle of the output voltage can be regulated. The mechanism of the pulse phase modulation was explained, and the PPM-controlled half-bridge resonant inverter was analyzed, and experimentally verified. The PPM control can be used to control the phase angles of the two-stage resonant inverters in a multiple resonant inverter system to reduce the circulating current, which is caused by phase discrepancy between modules. It can also be used in combination with PWM control to regulate both the phases and magnitudes of the output voltages, to minimize the circulating current in a multiple resonant inverter system. Experimental verification was presented with prototype resonant inverters of 100W, 500 kHz and output voltage 28V (RMS).

## References


[1] L. Massie, "Space power system requirements and issues: the next decade", *IEEE AES system magazine*, pp. 4–9, Dec. 1990.

[2] G. Ludwig, H. Wiegman, G. Claydon, R. Steigerwald, "100 kHz distributed power system for aircraft engine modular control", *Proceedings of IEEE Power Electronics Specialist Conference*, pp. 811–817, 1993.

[3] Kelley, "W. Owens, Contactor-less power supply for an aircraft passenger entertainment system", *IEEE Transactions on Power Electronics*, Vol. 4, No. 3, pp. 348–354, 1969.

[4] K. Woo, H. Park, Y. Cho, K. Kim, "Contact-less energy transmission system for linear servo motor", *IEEE Transactions on Magnetics*, Vol. 41, No. 5, pp. 1596–1599, May 2005.

[5] J. M. Barnard, J. A. Ferreria, J. D. van Wyk, "Sliding transformer for linear contact-less power delivery", *IEEE Trans. Industry Electronics*, Vol. 44, No. 6, pp. 774–779, Dec. 1997.

[6] D. A. G. Pedder, A. D. Brown, J. A. Skinner, "A contact-less electrical energy transmission system", *IEEE Trans. Industry Electronics*, Vol. 46, No. 1, pp. 23–30, Jan. 1999.

[7] Z. Ye, P. Jain, P. Sen, "Two Stage Resonant Inverter for AC Distributed Power Supplies, Full Control of Output Voltage Magnitude and Phase Angle", *Proceedings of 30th Annual Conference of IEEE Industrial Electronics Society*, Pusan, Korea, pp. 227–232, Nov. 2004.

[8] W. A. Tabisz, M. M. Jovanovic, F. C. Lee, "Present and future of distributed power systems", *Proceedings of 17th Annual Applied Power Electronics Conference and Exposition*, pp. 11–18, Feb. 1992.

[9] P. Lindman, L. Thorsell, "Applying distributed power modules in telecom systems", *IEEE Transactions on Power Electronics*, Vol. 11, No. 2, pp. 365–373, Mar. 1996.

[10] E. de la Cruz, S. Ollero, J. Rodriguez, J. Uceda, J. A. Cobos, "Review of suitable topologies for on-board DC/DC converters in distributed power architectures for telecom applications", *Proceeding of 14th International Telecommunications Energy Conference*, pp. 59–65, Oct. 1992.

[11] Z. Ye, P. Jain, P. Sen, "A two-stage resonant inverter featured with independent control of the phase angle and magnitude of the output voltage for multiple inverter applications", *IEEE Trans. on Industrial Electronics*, Vol. 54, No. 5, pp. 2797–2812, Oct. 2007.

[12] Z. Ye, P. Jain and P. Sen, "A full bridge resonant inverter with modified phase shift modulation", *Proceedings of 36th Annual IEEE Power Electronics Specialists Conference*, Recife, Brazil, pp. 642–649, 2005.

[13] Z. Ye, P. Jain, P. Sen, "A New Control Scheme for Circulating Current Minimization for High Frequency Multiple Inverter Modules Operated in Parallel", *Proceedings of 31st Annual Conference of IEEE Industrial Electronics Society*, Raleigh, NC, USA, pp. 992–999, Nov. 2005.

[14] J. A. Sabate, M. M. Jovanovic, F. C. Lee, R. Gean, "Analysis and design-optimization of LCC resonant inverter for high-frequency AC distributed power system", *IEEE*

*Transactions on Industrial Electronics*, Vol. 42, No. 1, pp. 63–71, Feb. 1995.

[15] Hamar. J., Nagy. I., "Asymmetrical operation of dual channel resonant DC-DC converters", *IEEE Transactions on Power Electronics*, Vol. 18, No. 1, Part 1, pp. 83–94, Jan. 2003.

[16] Z. Ye, P. Jain, P. Sen, "Analysis and Design of Full Bridge Resonant Inverter for High Frequency AC Distributed Power Supply Application", *Proceedings of 31st Annual Conference of IEEE Industrial Electronics Society*, Raleigh, NC, USA, pp. 1189–1196, Nov. 2005.

**Zhongming Ye** (M'01, SM'07) was born in Jiangsu, China. He received his PhD from Zhejiang University at Hangzhou, China, and Queen's University at Kingston, ON, Canada in 1998 and 2005, respectively. From 1998 to 1999, he worked in the Department of Electrical and Electronics Engineering at The University of Hong Kong, China. From 1999 to 2001, he worked in the Department of Electrical and Computer Engineering at Ryerson University, Toronto, ON, Canada. He is now an Applications Engineer, at Intersil, Milpitas, CA, USA. His fields of interest include high frequency power conversion, power electronics control, power distribution systems, electrical machine fault diagnostics, power quality, artificial intelligence, neural network and fuzzy logic. He has published over 70 papers on these topics in various peer reviewed journals and conferences. He is a Senior Member of IEEE, a member of the IEEE Power Electronics Society, and a member of the IEEE Industrial Electronics Society.

**Praveen K. Jain** (S'86, M'88, M'91, F'02) received his B.E. (Hons.) degree from the University of Allahabad, India, his M.A.Sc. and Ph.D. from the University of Toronto, Canada, in 1980, 1984, and 1987, respectively, all in Electrical Engineering. Presently, he is a Professor and Canada Research Chair in Power Electronics at Queen's University in Kingston, Ontario, Canada. From 1994 to 2000, he was a Professor at Concordia University, Montreal, Canada, where was engaged in teaching and research in the field of power electronics. Prior to this (1989-1994) he was a Technical Advisor with the Power Group, Nortel Networks, Ottawa, Canada, where he was providing guidance for research and development of advanced power technologies for telecommunications. During 1987-1989, he was with Canadian Astronautics Ltd., Ottawa, Canada, where he played a key role in the design and development of high frequency power conversion equipment for the Space Station Freedom. He was a design engineer and production engineer at Brown Boveri Company and Crompton Greaves Ltd., India, during 1980-1981. He also has considerable consulting experience within the industry. Dr. Jain has published over 250 technical papers and reports including 25 patents in the area of power electronics. His current research interests are power electronics applications for space, telecommunications and computer systems. He is a member of Professional Engineers of Ontario and an Associate Editor of IEEE Transactions on Power Electronics. He is the recipient of the 2004 Engineering Medal (R&D) of the Professional Engineers Ontario and is also a Fellow of the Engineering Institute of Canada.

**Paresh C. Sen** (M'67-SM'74-F'89) was born in Chittagong, Bangladesh. He received his B.Sc. degree (with honors in physics) and M.Sc. (Tech.) degree in applied physics from the University of Calcutta, India, in 1958 and 1961, respectively, and his M.A.Sc. and Ph.D. degrees in electrical engineering from the University of Toronto, Ontario, Canada, in 1965 and 1967, respectively. Presently, Dr. Sen is an Emeritus Professor of Electrical and Computer Engineering at Queen's University, Kingston, Ontario, Canada. He has written more than 160 research papers in the area of power electronics and drives. He is the author of two internationally acclaimed textbooks: *Principles of Electric Machines and Power Electronics* (New York: Wiley, 1989, 2nd ed., 1997) and *Thyristor DC Drives* (New York: Wiley, 1981). His fields of interest include power electronics, electric drive systems, switching power supplies, power factor correction circuits, modern control techniques for high performance drive systems, and applications of fuzzy logic control in power electronics and drive systems. Dr. Sen was the recipient of the IEEE Canada Outstanding Engineering Educator Award in 2006 for his outstanding contributions over four decades as an author, teacher, supervisor, researcher and consultant. He received the Prize Paper Award from the Industrial Drives Committee for technical excellence at the IEEE Industry Applications Society (IAS) Annual Meeting in 1986. Dr. Sen has served as an Associate Editor of the IEEE TRANSACTIONS ON INDUSTRIAL ELECTRONICS (1975-1982) and as Chairman of the Technical Committees on Power Electronics (1979-1980) and Energy Systems (1980-1982) of the IEEE Industrial Electronics Society. He served as an NSERC (Natural Science and Engineering Research Council of Canada) Scientific Liaison Officer evaluating University-Industry coordinated projects (1994-1999). As Emeritus Professor, Dr. Sen continues to be active in research, and in several IEEE societies.